Proceedings of the
Annual Stability Conference
Structural Stability Research Council
San Antonio, Texas, March 19-22, 2024

Inelastic stability of axially compressed CFS hollow stub columns with edge-stiffened perforations

M. Anbarasu[1], K. S. Vivek[2], Mohammad Adil Dar[3]

Abstract

Modular steel construction is increasingly popular due to its superior quality and speed. The structural stability of assembled modules relies on inter-module connections, but perforations in module columns, while providing access and services, affect compression members' capacity and stability. Edge-stiffened perforation has emerged as a viable solution, including for cold-formed steel (CFS) hollow stub columns. However, adopting plain and edge-stiffened perforations can alter stress distribution, ultimate strength, and post-buckling behavior. This study investigates the inelastic stability of axially compressed CFS hollow stub columns with edge-stiffened circular perforations. Numerical models of hollow stub columns are developed using ABAQUS and validated against relevant test results. Parametric studies are then conducted on non-perforated, plain perforated, and edge-stiffened perforated CFS square and rectangular hollow stub columns, considering different cross-sectional aspect ratios, sectional compactness, and perforation ratios. Circular perforations are centrally located at the mid-height of the columns. The numerical results are compared with predicted strengths using the current direct strength method (DSM) as per AISI S100-16 in the case of non-perforated and plain perforated columns. Providing edge-stiffened perforations resulted in greater axial capacity of stub columns in comparison to plain perforations. Interestingly, in columns with edge-stiffened perforations and a relatively high plate-slenderness ratio, the axial capacities exceeded those of corresponding non-perforated columns. The above findings clearly confirm the need for an extensive extended study for greater insight, to quantify the influencing parameters, and to propose modified design rules for stub columns provided with edge-stiffened perforations.

1. Introduction

Cold-formed steel (CFS) construction is widely adopted around the world owing to its lower dead load and ease of fabrication, connection at site, and erection. Contrary to the open sections (viz., channels and angles), the closed hollow (circular or rectangular) sections exhibit greater compressive strength and torsional stiffness. The hollow sections are generally preferred for

[1] Professor, Government College of Engineering, Dharmapuri, TN, India, < gceanbu@gmail.com>
[2] Asst. Professor, VVIT, AP, India, <saivivek@vvit.net>
[3] Marie Curie Fellow in Steel Structures, University of Sheffield, UK, <dar.adil@sheffield.ac.uk>

modular steel construction (MSC), in which the intra- and inter-modular connections are made by end plates (Ma et al. (2016); Singh & Chan 2021; Gatheesgar et al. 2021; Rajanayagam et al. 2021). The behaviour of square and rectangular hollow sections subjected to axial compression was reported earlier (Singh & Singh 2017, 2018; Shi et al. 2022). The sections with high plate-slenderness ratio were prone to local buckling. Yun & Gardner (2018) proposed direct strength method (DSM) procedure for design of tubular sections with non-slender elements. Liu et al. (2018) reported the design of space frame work comprised with tubular sections by adopting direct design method (DDM).

Perforations are required in the members to accommodate service ducts for satisfying various functional requirements. The cross-sectional elements of the CFS sections behave as thin plates under the action of compression. Several researchers (Yu & Davis 1973; Ritchie & Rhodes 1975; Roberts & Azizian 1984; Narayanan & Chow 1984; Shanmugham et al. 1999; Moen & Schafer 2009; Yao & Rasmussen 2012) investigated the stability and strength of axially compressed thin plates with perforations. The diameters or widths of circular, square, or rectangular perforations have a significant influence on the buckling capacity of the plates. In general, the buckling load decreases with an increase in perforation size. For thin-walled sections (such as channels) with perforations in the web plate, the width of the perforation is crucial in comparison to its length, as the length of the perforation does not reduce the width of the web plate. As the ratio of perforation size (the ratio of diameter to the width of the plate element) increased, the buckling load decreased.

Studies were reported on the axial behavior of lipped channel and hollow section columns with perforations in the literature (Kulatunga et al. 2003; Young et al. 2014; Feng et al. 2016; Kulatunga et al. 2014; Yao et al. 2016 a, b). The perforations resulted in reduced sectional capacity and led to localized failure (Singh & Chan 2021; Anbarasu et al. 2022). The introduction of perforations reduces the cross-sectional area, and the adjacent elements (at the level of perforation) become un-stiffened, which causes complex stress distribution resulting in reduced axial capacity (Moen & Schafer 2008, 2011).

2. Numerical modeling technique and validation

The finite element modeling and analysis of perforated tubes was carried out with the help of ABAQUS 6.14 software for validation and parametric studies (Anbarasu et al. 2022). A four-noded doubly curved shell element with reduced integration (S4R) was chosen. The element has 6 degrees of freedom (3 translations and 3 rotations with respect to the X, Y, and Z axes, respectively) at each node. The circular perforations were provided at the mid-length of the specimens. Shell elements with a size twice the thickness were assigned to the flat regions, and the curved corners were discretized into six elements. At the location of perforations, the flat was divided into 8 segments (i.e., the circumference of the circular perforation was divided into 8 segments). Further, each segment of the perforation was discretized with shell elements of size 3 mm to obtain a fine mesh upon several trails for convergence. A multi-point constraint (MPC) was created at either end of the specimen by creating reference points (RPs). The RP represents the centroid for the chosen size of cross-section. Concentric axial compression was applied by opting for displacement-controlled analysis. The material non-linearity (Gardener and Yun 2018) was incorporated into the models by inputting the true stress-strain values beyond the proportionality limit of the material for the flat and corner regions appropriately. The RIKS solver was chosen for performing non-linear buckling analysis (considering geometric non-linearity as well). The calibration of the numerical model was done by validating the test results of plain-perforated square and rectangular hollow sections available in the literature (Singh and Chan 2021). Table 1 presents the comparison of finite element analysis and available experimental results (Singh and Chan 2021). The mean and standard deviation of P_{EXP} / P_{FEA} were obtained as 1.03 and 0.04, respectively, indicating a decent match, and hence the adopted numerical modeling was extended for the parametric study.

Table 1: Comparison of test results and numerical strengths for validation (Singh & Chan 2021)

S. No.	Specimen ID	P_{EXP} (kN)	P_{FEA} (kN)	P_{EXP} / P_{FEA}
1	80 x 40 x 2.6d/w0.1-1	323.49	319.36	1.01
2	80 x 40 x 2.6d/w0.3-1	290.18	272.86	1.06
3	80 x 40 x 2.6d/w0.7-1	211.93	194.76	1.09
4	50 x 50 x 2.9d/w0.5-1	207.99	202.87	1.03
5	50 x 50 x 2.9d/w0.7-1	187.16	183.27	1.02
6	50 x 50 x 2.9d/w0.9-1	159.44	162.54	0.98
	Mean			1.03
	Std. Dev.			0.04

3. Parametric study

For the purpose of a comprehensive parametric study, analysis was carried out for square (B = D = 100 mm) and rectangular (B = 100 mm and D = 200 mm) hollow sections (SHS and RHS, respectively) for the cases of no perforation (NP), plain perforation (PP), and edge-stiffened perforations (SP), where 'B' and 'D' are the overall width and depth of the sections, respectively, as shown in Figure 1(a). The D/B is 1.0 and 2.0 for square and rectangular sections, respectively. Further, four different thicknesses (1.5 mm, 2.0 mm, 3.0 mm, and 4.0 mm) were assumed for each section to account for plate-slenderness ratio (λ_p). The length of all the specimens was assumed to be 400 mm in order to be categorized as 'stub' columns. The ratio of the diameter (d) of the perforation to the plate width (w) was varied from 0.5 to 0.9 with an interval of 0.1 to account for the size effect of the perforation. The geometric details of the considered specimens are presented in Table 2. For the edge-stiffened perforation, the radius and length of the lip were assumed to be 3 mm and 10 mm, respectively, as depicted in Figure 1(b). The nomenclature used for the specimen ID was explained in Figure 2. The material properties considered for the flat and corner regions of the specimens were presented in Table 3. Local imperfections were incorporated (Anbarasu et al., 2022) in all the models appropriately.

4. Design strength

Provisions for determining the strength of non-perforated and perforated compression members are available in the current specification of North America (AISI S100-16).

$$P_{nl} = \begin{cases} P_{ne} & for\ \lambda_l \leq 0.776 \\ \left[1 - 0.15\left(\frac{P_{crl}}{P_{ne}}\right)^{0.4}\right]\left(\frac{P_{crl}}{P_{ne}}\right)^{0.4} P_{ne} & for\ \lambda_l > 0.776 \end{cases} \quad (1)$$

Table 2: Dimensions

Specimen ID	B (mm)	D (mm)	r_i (mm)	r_f (mm)	t (mm)	w (mm)	d (mm)	d_o (mm)	L_l (mm)
NP_100 x 100 x 1.5	100	100	2.25	-	1.5	92.50	00.00	-	-
PP_100 x 100 x 1.5 - 0.5	100	100	2.25	-	1.5	92.50	46.25	-	-
SP_100 x 100 x 1.5 - 0.5	100	100	2.25	3	1.5	92.50	46.25	52.25	10
PP_100 x 100 x 1.5 - 0.6	100	100	2.25	-	1.5	92.50	55.50	-	-
SP_100 x 100 x 1.5 - 0.6	100	100	2.25	3	1.5	92.50	55.50	61.50	10
PP_100 x 100 x 1.5 - 0.7	100	100	2.25	-	1.5	92.50	64.75	-	-
SP_100 x 100 x 1.5 - 0.7	100	100	2.25	3	1.5	92.50	64.75	70.75	10
PP_100 x 100 x 1.5 - 0.8	100	100	2.25	-	1.5	92.50	74.00	-	-
SP_100 x 100 x 1.5 - 0.8	100	100	2.25	3	1.5	92.50	74.00	80.00	10
PP_100 x 100 x 1.5 - 0.9	100	100	2.25	-	1.5	92.50	83.25	-	-
SP_100 x 100 x 1.5 - 0.9	100	100	2.25	3	1.5	92.50	83.25	89.25	10
NP_100 x 100 x 2.0	100	100	3.00	-	2.0	90.00	00.00	-	-
PP_100 x 100 x 2.0 - 0.5	100	100	3.00	-	2.0	90.00	45.00	-	-
SP_100 x 200 x 2.0 - 0.5	100	100	3.00	3	2.0	90.00	45.00	51.00	10
PP_100 x 100 x 2.0 - 0.6	100	100	3.00	-	2.0	90.00	54.00	-	-
SP_100 x 100 x 2.0 - 0.6	100	100	3.00	3	2.0	90.00	54.00	60.00	10
PP_100 x 100 x 2.0 - 0.7	100	100	3.00	-	2.0	90.00	63.00	-	-
SP_100 x 100 x 2.0 - 0.7	100	100	3.00	3	2.0	90.00	63.00	69.00	10
PP_100 x 100 x 2.0 - 0.8	100	100	3.00	-	2.0	90.00	72.00	-	-
SP_100 x 100 x 2.0 - 0.8	100	100	3.00	3	2.0	90.00	72.00	78.00	10
PP_100 x 100 x 2.0 - 0.9	100	100	3.00	-	2.0	90.00	81.00	-	-
SP_100 x 100 x 2.0 - 0.9	100	100	3.00	3	2.0	90.00	81.00	87.00	10
NP_100 x 100 x 3.0	100	100	4.50	-	3.0	85.00	00.00	-	-
PP_100 x 100 x 3.0-0.5	100	100	4.50	-	3.0	85.00	42.50	-	-
SP_100 x 100 x 3.0-0.5	100	100	4.50	3	3.0	85.00	42.50	48.50	10
PP_100 x 100 x 3.0-0.6	100	100	4.50	-	3.0	85.00	51.00	-	-
SP_100 x 100 x 3.0-0.6	100	100	4.50	3	3.0	85.00	51.00	57.00	10
PP_100 x 100 x 3.0-0.7	100	100	4.50	-	3.0	85.00	59.50	-	-
SP_100 x 100 x 3.0-0.7	100	100	4.50	3	3.0	85.00	59.50	65.50	10
PP_100 x 100 x 3.0-0.8	100	100	4.50	-	3.0	85.00	68.00	-	-
SP_100 x 100 x 3.0-0.8	100	100	4.50	3	3.0	85.00	68.00	74.00	10
PP_100 x 100 x 3.0-0.9	100	100	4.50	-	3.0	85.00	76.50	-	-
SP_100 x 100 x 3.0-0.9	100	100	4.50	3	3.0	85.00	76.50	82.50	10
NP_100 x 100 x 4.0	100	100	6.00	-	4.0	80.00	00.00	-	-
PP_100 x 100 x 4.0-0.5	100	100	6.00	-	4.0	80.00	40.00	-	-

Specimen ID	B (mm)	D (mm)	r_i (mm)	r_f (mm)	t (mm)	w (mm)	d (mm)	d_o (mm)	L_l (mm)
SP_100 x 100 x 4.0-0.5	100	100	6.00	3	4.0	80.00	40.00	46.00	10
PP_100 x 100 x 4.0-0.6	100	100	6.00	-	4.0	80.00	48.00	-	-
SP_100 x 100 x 4.0-0.6	100	100	6.00	3	4.0	80.00	48.00	54.00	10
PP_100 x 100 x 4.0-0.7	100	100	6.00	-	4.0	80.00	56.00	-	-
SP_100 x 100 x 4.0-0.7	100	100	6.00	3	4.0	80.00	56.00	62.00	10
PP_100 x 100 x 4.0-0.8	100	100	6.00	-	4.0	80.00	64.00	-	-
SP_100 x 100 x 4.0-0.8	100	100	6.00	3	4.0	80.00	64.00	70.00	10
PP_100 x 100 x 4.0-0.9	100	100	6.00	-	4.0	80.00	72.00	-	-
SP_100 x 100 x 4.0-0.9	100	100	6.00	3	4.0	80.00	72.00	78.00	10
PP_100 x 200 x 1.5-0.5	100	200	2.25	-	1.5	192.50	96.25	-	-
SP_100 x 200 x 1.5-0.5	100	200	2.25	3	1.5	192.50	96.25	102.25	10
PP_100 x 200 x 1.5-0.6	100	200	2.25	-	1.5	192.50	115.50	-	-
SP_100 x 200 x 1.5-0.6	100	200	2.25	3	1.5	192.50	115.50	121.50	10
PP_100 x 200 x 1.5-0.7	100	200	2.25	-	1.5	192.50	134.75	-	-
SP_100 x 200 x 1.5-0.7	100	200	2.25	3	1.5	192.50	134.75	140.75	10
PP_100 x 200 x 1.5-0.8	100	200	2.25	-	1.5	192.50	154.00	-	-
SP_100 x 200 x1.5-0.8	100	200	2.25	3	1.5	192.50	154.00	160.00	10
PP_100 x 200 x 1.5-0.9	100	200	2.25	-	1.5	192.50	173.25	-	-
SP_100 x 200 x 1.5-0.9	100	200	2.25	3	1.5	192.50	173.25	179.25	10
PP_100 x 200 x 2.0-0.5	100	200	3.00	-	2.0	190.00	95.00	-	-
SP_100 x 200 x 2.0-0.5	100	200	3.00	3	2.0	190.00	95.00	101.00	10
PP_100 x 200 x 2.0-0.6	100	200	3.00	-	2.0	190.00	114.00	-	-
SP_100 x 200 x 2.0-0.6	100	200	3.00	3	2.0	190.00	114.00	120.00	10
PP_100 x 200 x 2.0-0.7	100	200	3.00	-	2.0	190.00	133.00	-	-
SP_100 x 200 x 2.0-0.7	100	200	3.00	3	2.0	190.00	133.00	139.00	10
PP_100 x 200 x 2.0-0.8	100	200	3.00	-	2.0	190.00	152.00	-	-
SP_100 x 200 x 2.0-0.8	100	200	3.00	3	2.0	190.00	152.00	158.00	10
PP_100 x 200 x 2.0-0.9	100	200	3.00	-	2.0	190.00	171.00	-	-
SP_100 x 200 x 2.0-0.9	100	200	3.00	3	2.0	190.00	171.00	177.00	10
PP_100 x 200 x 3.0-0.5	100	200	4.50	-	3.00	185.00	92.50	-	-
SP_100 x 200 x 3.0-0.5	100	200	4.50	3	3.00	185.00	92.50	98.50	10
PP_100 x 200 x 3.0-0.6	100	200	4.50	-	3.00	185.00	92.50	-	-
SP_100 x 200 x 3.0-0.6	100	200	4.50	3	3.00	185.00	111.00	117.00	10
PP_100 x 200 x 3.0-0.7	100	200	4.50	-	3.00	185.00	129.50	-	-
SP_100 x 200 x 3.0-0.7	100	200	4.50	3	3.00	185.00	129.50	135.50	10
PP_100 x 200 x 3.0-0.8	100	200	4.50	-	3.00	185.00	148.00	-	-
SP_100 x 200 x 3.0-0.8	100	200	4.50	3	3.00	185.00	148.00	154.00	10

Specimen ID	B (mm)	D (mm)	r_i (mm)	r_f (mm)	t (mm)	w (mm)	d (mm)	d_o (mm)	L_l (mm)
PP_100 x 200 x3.0-0.9	100	200	4.50	-	3.00	185.00	166.50	-	-
SP_100 x 200 x 3.0-0.9	100	200	4.50	3	3.0	185.00	166.50	172.50	10
PP_100 x 200 x 4.0-0.5	100	200	6.00	-	4.0	180.00	90.00	-	-
SP_100 x 200 x 4.0-0.5	100	200	6.00	3	4.0	180.00	90.00	96.00	10
PP_100 x 200 x 4.0-0.6	100	200	6.00	-	4.0	180.00	108.00	-	-
SP_100 x 200 x 4.0-0.6	100	200	6.00	3	4.0	180.00	108.00	114.00	10
PP_100 x 200 x 4.0-0.7	100	200	6.00	-	4.0	180.00	126.00	-	-
SP_100 x 200 x 4.0-0.7	100	200	6.00	3	4.0	180.00	126.00	132.00	10
PP_100 x 200 x 4.0-0.8	100	200	6.00	-	4.0	180.00	144.00	-	-
SP_100 x 200 x 4.0-0.8	100	200	6.00	3	4.0	180.00	144.00	150.00	10
PP_100 x 200 x 4.0-0.9	100	200	6.00	-	4.0	180.00	162.00	-	-
SP_100 x 200 x 4.0-0.9	100	200	6.00	3	4.0	180.00	162.00	168.00	10

Table 3: Material property

Material property	Flat	Corner
Modulus of elasticity, E (MPa)	213860	210000
Yield stress, f_y (MPa)	482.50	572.07
Ultimate stress, f_u (MPa)	588.90	609.08

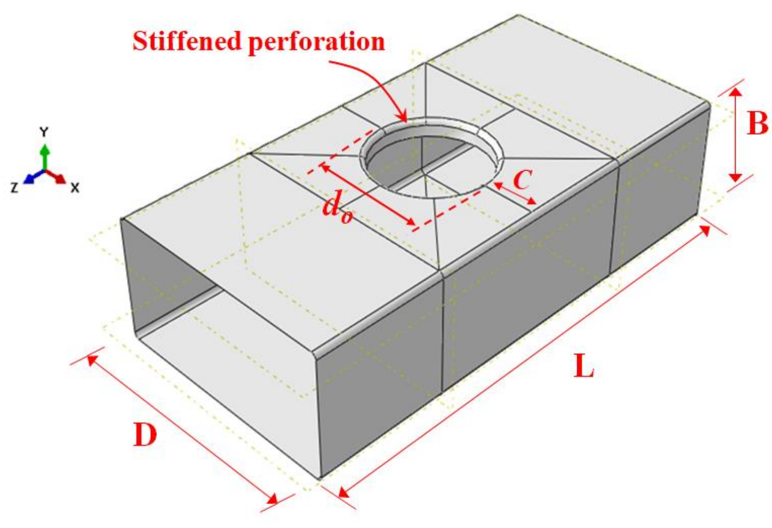

a. Isometric view

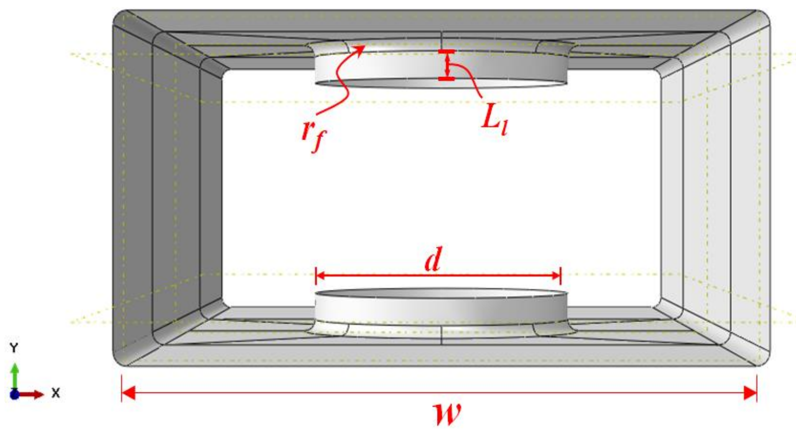

b. Side view

Figure 1: Tube with edge-stiffened perforation

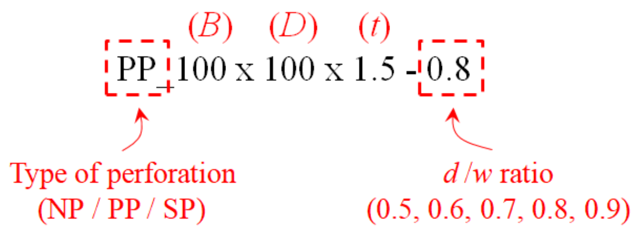

Figure 2: Nomenclature

$$\text{where } \lambda_l = \sqrt{P_{ne}/P_{crl}} \tag{2}$$

For plain perforated sections, $P_{nl} \leq P_{y,net}$

$$\text{Where } P_{y,net} = A_n * f_y \tag{3}$$

A_n = net area

f_y = yield stress

The nominal axial capacity (P_{ne}) for yielding and global buckling can be determined from

$$P_{ne} = \begin{cases} \left(0.658^{\lambda_c{}^2}\right) P_y & for\, \lambda_c \leq 1.5 \\ \left(\dfrac{0.877}{\lambda_c^2}\right) P_y & for\, \lambda_c \leq 1.5 \end{cases} \tag{4}$$

$$\text{Where } \lambda_c = \sqrt{P_y/P_{cr,e}} \tag{5}$$

The elastic global buckling load ($P_{cr,e}$) is calculated as per Appendix 2 of AISI S100-16. However, no provisions for edge-stiffened perforations were available.

Table 4: Results for SHS (100 x 100) stub columns

Sl.No.	Specimen ID	λ_p	λ_l	$\frac{P_{FEA}}{P_{y,net}}$	$\frac{P_{FEA}}{P_{FEA\_NP}}$	$\frac{P_{FEA}}{P_{n,DSM}}$
1	NP_100 x 100 x 1.5	2.944	1.65	0.49	1.00	0.81
2	PP_100 x 100 x 1.5-0.5	0.894	1.90	0.63	0.98	0.88
3	SP_100 x 100 x 1.5-0.5	0.751	-	0.56	1.02	-
4	PP_100 x 100 x 1.5-0.6	0.778	1.95	0.64	0.93	0.85
5	SP_100 x 100 x 1.5-0.6	0.635	-	0.58	1.01	-
6	PP_100 x 100 x 1.5-0.7	0.663	2.02	0.64	0.87	0.82
7	SP_100 x 100 x 1.5-0.7	0.519	-	0.60	0.99	-
8	PP_100 x 100 x 1.5-0.8	0.547	2.10	0.62	0.78	0.75
9	SP_100 x 100 x 1.5-0.8	0.404	-	0.59	0.91	-
10	PP_100 x 100 x 1.5-0.9	0.431	2.18	0.60	0.70	0.69
11	SP_100 x 100 x 1.5-0.9	0.288	-	0.56	0.81	-
12	NP_100 x 100 x 2.0	2.152	1.23	0.60	1.00	0.81
13	PP_100 x 100 x 2.0-0.5	0.653	1.41	0.73	0.94	0.84
14	SP_100 x 100 x 2.0-0.5	0.534	-	0.67	1.02	-
15	PP_100 x 100 x 2.0-0.6	0.569	1.45	0.75	0.91	0.82
16	SP_100 x 100 x 2.0-0.6	0.449	-	0.70	1.00	-
17	PP_100 x 100 x 2.0-0.7	0.484	1.50	0.76	0.85	0.79
18	SP_100 x 100 x 2.0-0.7	0.365	-	0.70	0.95	-
19	PP_100 x 100 x 2.0-0.8	0.400	1.56	0.74	0.78	0.75
20	SP_100 x 100 x 2.0-0.8	0.280	-	0.68	0.87	-
21	PP_100 x 100 x 2.0-0.9	0.315	1.62	0.72	0.70	0.72
22	SP_100 x 100 x 2.0-0.9	0.196	-	0.66	0.80	-
23	NP_100 x 100 x 3.0	0.680	0.82	0.80	1.00	0.83
24	PP_100 x 100 x 3.0-0.5	0.413	0.94	0.94	0.91	0.94
25	SP_100 x 100 x 3.0-0.5	0.317	-	0.86	0.97	-
26	PP_100 x 100 x 3.0-0.6	0.359	0.97	0.93	0.85	0.93
27	SP_100 x 100 x 3.0-0.6	0.263	-	0.86	0.92	-
28	PP_100 x 100 x 3.0-0.7	0.306	1.00	0.97	0.83	0.97
29	SP_100 x 100 x 3.0-0.7	0.210	-	0.85	0.87	-
30	PP_100 x 100 x 3.0-0.8	0.253	1.04	0.93	0.74	0.93
31	SP_100 x 100 x 3.0-0.8	0.157	-	0.84	0.81	-
32	PP_100 x 100 x 3.0-0.9	0.199	1.08	0.92	0.68	0.92
33	SP_100 x 100 x 3.0-0.9	0.103	-	0.83	0.75	-
34	NP_100 x 100 x 4.0	0.482	0.61	0.92	1.00	0.92
35	PP_100 x 100 x 4.0-0.5	0.292	0.69	1.01	0.86	1.01
36	SP_100 x 100 x 4.0-0.5	0.208	-	0.93	0.93	-
37	PP_100 x 100 x 4.0-0.6	0.255	0.70	1.05	0.84	1.05
38	SP_100 x 100 x 4.0-0.6	0.170	-	0.90	0.86	-
39	PP_100 x 100 x 4.0-0.7	0.217	0.73	1.00	0.76	1.00
40	SP_100 x 100 x 4.0-0.7	0.133	-	0.91	0.83	-
41	PP_100 x 100 x 4.0-0.8	0.179	0.75	1.07	0.76	1.07
42	SP_100 x 100 x 4.0-0.8	0.095	-	0.91	0.78	-
43	PP_100 x 100 x 4.0-0.9	0.141	0.78	0.99	0.66	0.99
44	SP_100 x 100 x 4.0-0.9	0.057	-	0.93	0.73	-

Table 5: Results for RHS (100 x 200) stub columns

Sl.No.	Specimen ID	λ_p	λ_l	$\frac{P_{FEA}}{P_{y,net}}$	$\frac{P_{FEA}}{P_{FEA\_NP}}$	$\frac{P_{FEA}}{P_{n,DSM}}$
1	NP_100 x 200 x 1.5	3.058	2.85	0.39	1.00	0.96
2	PP_100 x 200 x 1.5-0.5	1.857	3.47	0.52	0.91	1.01
3	SP_100 x 200 x 1.5-0.5	1.714	-	0.52	1.03	-
4	PP_100 x 200 x 1.5-0.6	1.617	3.66	0.57	0.89	1.03
5	SP_100 x 200 x 1.5-0.6	1.474	-	0.68	1.08	-
6	PP_100 x 200 x 1.5-0.7	1.377	3.87	0.57	0.81	0.97
7	SP_100 x 200 x 1.5-0.7	1.234	-	0.61	1.01	-
8	PP_100 x 200 x 1.5-0.8	1.137	4.13	0.59	0.73	0.93
9	SP_100 x 200 x 1.5-0.8	0.994	-	0.63	0.92	-
10	PP_100 x 200 x 1.5-0.9	0.896	4.44	0.61	0.65	0.87
11	SP_100 x 200 x 1.5-0.9	0.753	-	0.59	0.76	-
12	NP_100 x 200 x 2.0	2.266	2.13	0.49	1.00	0.97
13	PP_100 x 200 x 2.0-0.5	1.376	2.59	0.62	0.87	0.97
14	SP_100 x 200 x 2.0-0.5	1.257	-	0.66	1.04	-
15	PP_100 x 200 x 2.0-0.6	1.198	2.73	0.67	0.84	0.98
16	SP_100 x 200 x 2.0-0.6	1.079	-	0.73	1.05	-
17	PP_100 x 200 x 2.0-0.7	1.020	2.89	0.70	0.78	0.95
18	SP_100 x 200 x 2.0-0.7	0.901	-	0.72	0.94	-
19	PP_100 x 200 x 2.0-0.8	0.842	3.07	0.71	0.71	0.90
20	SP_100 x 200 x 2.0-0.8	0.723	-	0.72	0.84	-
21	PP_100 x 200 x 2.0-0.9	0.664	3.31	0.72	0.62	0.83
22	SP_100 x 200 x 2.0-0.9	0.545	-	0.67	0.70	-
23	NP_100 x 200 x 3.0	1.474	1.41	0.66	1.00	0.98
24	PP_100 x 200 x 3.0-0.5	0.895	1.71	0.84	0.87	0.97
25	SP_100 x 200 x 3.0-0.5	0.800	-	0.89	1.04	-
26	PP_100 x 200 x 3.0-0.6	0.780	1.80	0.95	0.90	1.04
27	SP_100 x 200 x 3.0-0.6	0.684	-	0.92	0.99	-
28	PP_100 x 200 x 3.0-0.7	0.664	1.90	0.90	0.76	0.92
29	SP_100 x 200 x 3.0-0.7	0.568	-	0.89	0.87	-
30	PP_100 x 200 x 3.0-0.8	0.548	2.02	0.84	0.63	0.84
31	SP_100 x 200 x 3.0-0.8	0.452	-	0.89	0.78	-
32	PP_100 x 200 x 3.0-0.9	0.432	2.17	0.98	0.63	0.98
33	SP_100 x 200 x 3.0-0.9	0.337	-	0.83	0.65	-
34	NP_100 x 200 x 4.0	1.078	1.05	0.77	1.00	0.94
35	PP_100 x 200 x 4.0-0.5	0.655	1.54	0.98	0.86	1.06
36	SP_100 x 200 x 4.0-0.5	0.571	-	0.98	0.98	-
37	PP_100 x 200 x 4.0-0.6	0.570	1.69	1.02	0.82	1.08
38	SP_100 x 200 x 4.0-0.6	0.486	-	0.98	0.91	-
39	PP_100 x 200 x 4.0-0.7	0.485	1.89	1.07	0.77	1.09
40	SP_100 x 200 x 4.0-0.7	0.402	-	0.98	0.83	-
41	PP_100 x 200 x 4.0-0.8	0.401	2.13	1.08	0.69	1.08
42	SP_100 x 200 x 4.0-0.8	0.317	-	0.95	0.72	-
43	PP_100 x 200 x 4.0-0.9	0.316	2.44	1.03	0.58	1.03
44	SP_100 x 200 x 4.0-0.9	0.232	-	0.92	0.62	-

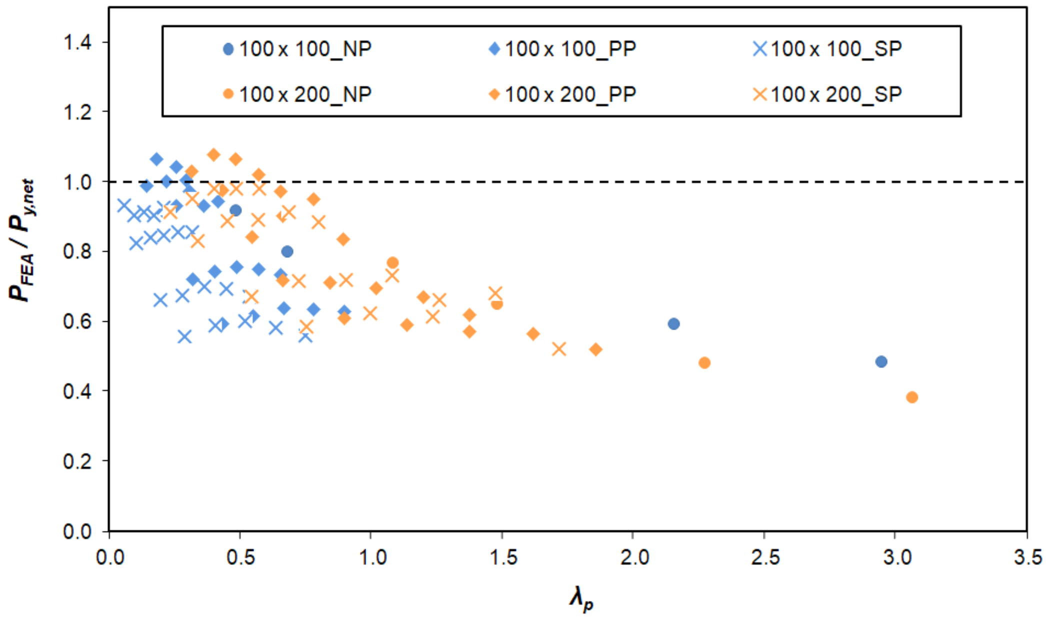

Figure 3: '$P_{FEA} / P_{y,net}$' vs 'λ_p'

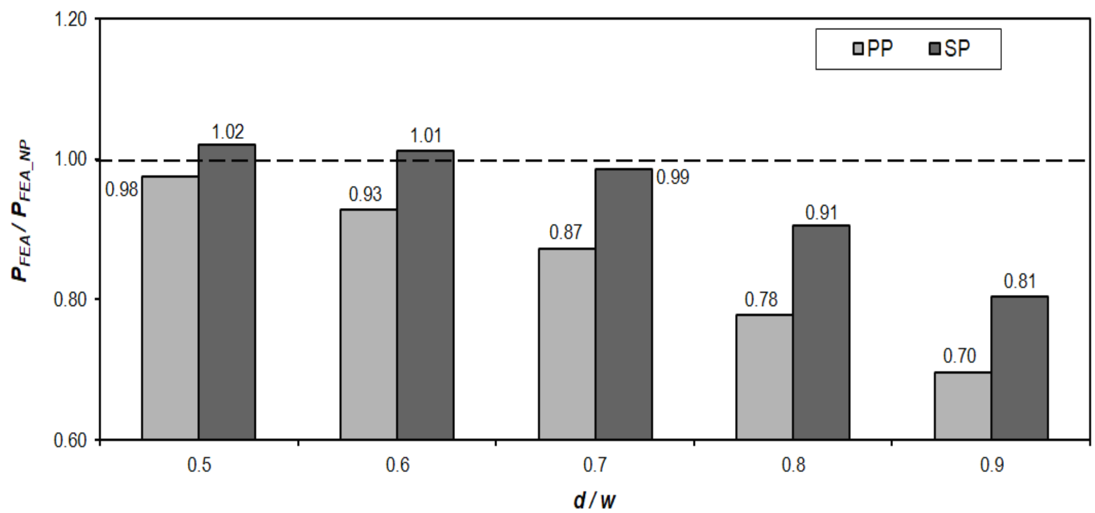

Figure 4: 'P_{FEA} / P_{FEA_NP}' vs 'd / w' for 100 x 100 x 1.5 (SHS) stub column

Assuming simply supported boundary condition, the plate slenderness ratio (λ_p) at the location of perforation can be calculated from

$$\lambda_p = (c / t) * \sqrt{\frac{f_y}{E}} \tag{6}$$

where, c = equivalent un-stiffened plate element on either side of the perforation (Figure 1(a))

$$= \frac{w}{2} - \frac{\pi * d}{8} \tag{7}$$

5. Results and Discussion

The numerical axial capacities (P_{FEA}) of SHS (100 x 100) and RHS (100 x 200) were presented in Tables 4 and 5, respectively. The nominal capacities as per DSM ($P_{n,DSM}$) of AISI S100-26 were also presented for the plain non-perforated and plain perforated members. The following observations are made upon careful examination of the obtained results:

1) In general, providing edge-stiffened perforations resulted in greater axial capacity (P_{FEA}) of the stub columns in comparison to the plain perforations, irrespective of the *d/w* ratio and λ_p in both the SHS and RHS.

2) In the case of edge-stiffened perforations and relatively higher plate slenderness (λ_p), the column axial strengths were surprisingly found to be slightly greater in comparison to the corresponding non-perforated sections (see Tables 4-5 and Figure 4).

3) In SHS, plain-perforated sections possessed higher P_{FEA} / $P_{y,net}$ in comparison to the edge-stiffened perforated sections. However, vice versa was observed for the RHS in the majority of cases.

6. Conclusions

In this study, the influence of edge-stiffened perforation on the axial capacity of the CFS hollow stub columns in comparison to non-perforated and plain perforated sections was investigated by performing non-linear finite element buckling analysis. Initially, a numerical model was developed in ABAQUS software. The model was validated with the available test data from the literature. As the obtained numerical results were in good agreement with the test results, the same modeling procedure was extended to carry out a parametric study. Non-perforated, plain perforated, and edge-stiffened perforated CFS square and rectangular hollow section (SHS and RHS, respectively) stub columns, considering different sectional compactness and perforation ratios, were modeled and analyzed. The obtained numerical axial capacities of the non-perforated and plain perforated columns were also compared with the available direct strength method (DSM) design provisions of AISI S100-16. Greater axial capacity was exhibited by the stub hollow columns with edge-stiffened perforations in comparison to plain perforations in all the considered cases. Surprisingly, the axial capacities of stub columns provided with edge-stiffened perforations and of relatively higher plate slenderness were found to exceed the capacity of non-perforated columns. A further extensive study is required to gather more data for performing reliability analysis in accurate quantification of the influencing parameters and to propose new or modified DSM provisions for the design of stub hollow columns with edge-stiffened perforations.

References

AISI S100-16 North American specification for the design of cold-formed steel structural members. Washington, DC: American Iron and Steel Institute; 2016.

Anbarasu, M., Subalakshmi, M., Dar, M. A., Hassanein, M. F. (2022). "Cold-formed ferritic stainless steel perforated tubular stub columns: Behaviour and design." *Thin-Walled Structures*, 170, 108654.

Feng, R., Mou, X., Chen, A., Ma, Y. (2016). "Tests of aluminium alloy CHS columns with circular openings", *Thin-Walled Structures*, 109, 113-131.

Gardner, L., Yun, X. (2018). "Description of stress-strain curves for cold-formed steels." *Construction and Building Materials*, 189, 527-538.

Gatheesgar, P., Poologanathan, K., Gunalan, S., Shyha, I., Sherlock, P., Rajanayagam, H., Nagaratnam, B. (2021).

"Development of affordable steel-framed modular buildings for emergency situations (Covid-19)." Structures, 31, 862-875.
Kulatunga, M. P., Macdonald, M. (2003). "Investigation of cold-formed steel structural members with perforations of different arrangements subjected to compression loading.", *Thin-Walled Structures*, 67, 78-87.
Kulatunga, M. P., Macdonald, M., Rhodes, J., Harrison, D. K. (2014). "Load capacity of cold-formed column members of lipped channel cross-section with perforations subjected to compression loading – Part I: FE simulation and test results." *Thin-Walled Structures*, 80, 1-12.
Liu, W., Zhang, H., Rasmussen, K. (2018). "Direct Design Method for space frames with cold-formed steel hollow sections." *Engineering Structures*, 166, 79-92.
Ma, J., -L., Chan, T. –M., Young, B. (2016). "Experimental investigation on stub-column behaviour of cold-formed high-strength steel tubular sections." *Journal of Structural Engineering, ASCE*, 142, 4015174.
Moen, C. D., Schafer, B. W. (2008). "Experiments on cold-formed steel columns with holes." *Thin-Walled Structures*, 46, 1164-1182.
Moen, C. D., Schafer, B. W. (2009). "Elastic buckling of thin plates with holes in compression or bending." *Thin-Walled Structures*, 47, 1597-1607.
Moen, C. D., Schafer, B. W. (2011). "Direct strength method for design of cold-formed steel columns with holes." *Journal of Structural Engineering, ASCE*, 46, 1164-1182.
Narayanan, R., Chow, F. Y. (1984). "Ultimate capacity of uni-axially compressed perforated plates." *Thin-Walled Structures*, 2, 241-264.
Rajanayagam, H., Poologanathan, K., Gatheesgar, P., Varelis, G. E., Sherlock, P., Nagaratnam, B., Hackney, P. (2021). "A-State-Of-The-Art review on modular building connections." *Structures*, 34, 1903-1922.
Ritchie, D., Rhodes, J. (1975). "Buckling and post-buckling of plates with holes." *Aeronautical Quarterly*, 26, 281-296.
Roberts, T. M., Azizian, Z. G. (1984). "Strength of perforated plates subjected to in-plane loading." *Thin-Walled Structures*, 2, 153-164.
Shanmugam, N. E., Thevendran, V., Tan, Y. H. (1999). "Design formula for axially compressed perforated plates", *Thin-Walled Structures*, 34, 1-20.
Shi, X., Cheng, X., Wang, X., Mansour, M. (2022). "Ultimate Behaviour and Design of Cold-formed Steel Square Hollow Section Members." *International Journal of Steel Structures*, 22, 767-790
Singh, T. G., Singh, K. D. (2017). "Structural performance of YSt–310 cold–formed tubular steel stub columns." *Thin-Walled Structures*, 121, 25-40.
Singh, T. G., Singh, K. D. (2018). "Experimental investigation on performance of perforated cold–formed steel tubular stub columns." *Thin-Walled Structures*, 131, 107-121.
Singh, T. G., Chan, T, M. (2021). "Effect of access openings on the buckling performance of square hollow section module stub columns." *Journal of Constructional Steel Research*, 177, 106438.
Yao, Z., Rasmussen, K. J. R. (2012). "Inelastic local buckling behaviour of perforated plates and sections under compression." *Thin-Walled Structures*, 61, 49-70.
Yao, Z., Rasmussen, K. J. R. (2016, a). "Perforated cold-formed steel members in compression I: parametric studies." *Journal of Structural Engineering, ASCE*, 143, 4016226.
Yao, Z., Rasmussen, K. J. R. (2016, b). "Perforated cold-formed steel members in compression II: Design." *Journal of Structural Engineering, ASCE*, 143, 4016227.
Young, B. K., Gap, D. K., In, K. K. (2014). "Compression tests of cold-formed channel sections with perforations in the web.", *Steel and Composite Structures*, 16, 657-679.
Yu, W. W., Davis, C. S. (1973). "Cold-formed steel members with perforated elements." *Journal of the Structural Divison, ASCE*, 99, 2061-2077.
Yun, X., Gardner, L. (2018). "The continuous strength method for the design of cold-formed steel non-slender tubular cross-sections." *Engineering Structures*, 175, 549-564.